



Ultrafast carrier transfer evidencing graphene electromagnetically enhanced ultrasensitive SERS in graphene/Ag-nanoparticles hybrid



Yujin Wang ^{a,1}, Hailong Chen ^{a,1}, Mengtao Sun ^c, Zehan Yao ^a, Baogang Quan ^a, Zhe Liu ^a, Yuxiang Weng ^{a,b}, Jimin Zhao ^{a,**}, Changzhi Gu ^{a,b,***}, Junjie Li ^{a,b,*}

^a Beijing National Laboratory for Condensed Matter Physics, Institute of Physics, Chinese Academy of Sciences, Beijing 100190, PR China

^b School of Physical Sciences, CAS Key Laboratory of Vacuum Physics, University of Chinese Academy of Sciences, Beijing 100190, PR China

^c Beijing Key Laboratory for Magneto-Photoelectrical Composite and Interface Science, School of Mathematics and Physics, University of Science and Technology Beijing, Beijing 100083, PR China

ARTICLE INFO

Article history:

Received 31 March 2017

Received in revised form

5 May 2017

Accepted 22 May 2017

Available online 18 June 2017

Keywords:

Ultrafast carrier transfer

Electromagnetic enhancement

Ultrasensitive SERS

Graphene/Ag-nanoparticles hybrid

ABSTRACT

Graphene-metal hybrid systems are highly promising as a very important building block in plasmonic structure for biosensing and catalyzing applications. However, the potential and mechanism of graphene in plasmon enhancement for such hybrids are not clear enough, although the corresponding enhancement of light-matter interaction has been reported. Here, we report an ultrafast optical spectroscopy investigation of a graphene/Ag-nanoparticles (NP) hybrid structure and evidence photo-carrier transfer from graphene to the Ag-NP. More importantly, we show that the graphene layer acts as an electron reservoir, and the electrons that transfer from it to the Ag-NP greatly enhance plasmon excitations therein, thereby generating giant local electromagnetic field enhancement in its hybrid. Further, we show that this graphene-derived local electromagnetic enhancement contributes greatly to ultrasensitive (10^{-13} M) surface-enhanced Raman scattering (SERS) in this hybrid. Our investigation reveals graphene's electromagnetic enhancement of SERS by uncovering an ultrafast carrier transfer mechanism in the graphene-plasmonic hybrid, and these results pave the way for the development of ultrasensitive plasmonic devices.

© 2017 Elsevier Ltd. All rights reserved.

1. Introduction

Since its discovery in 2004, graphene, the precursor of many interesting two-dimensional (2D) materials [1–3], has been investigated extensively owing to its superb electronic [4], optical [5], acoustic [6], and mechanical [7] properties. A pristine graphene layer exhibits broadband tunable, unusually high (up to 2.3% over the visible/near-IR range) light absorption [8], which exhibits strong light-carrier interaction that fosters vast promising applications in photonics and optoelectronics. Recently, hybrid systems

of graphene with metal nanostructures have attracted growing interests in both theoretical [9,10] and experimental [11–15] investigations. Versatile conventional metallic nanostructures ranging from nanoparticles [16–18] to plasmonic metamaterials [19,20] have been shown to provide an effective platform to enhance the excellent properties of graphene. For example, graphene-plasmonic hybrid devices are promising for various chemical or biological detection [21–23], photo-detection [5,6], and photocatalysis procedures [24–26]. However, the physical mechanism underlying the interaction between the graphene carriers and the noble metal plasmon remains a subject of debate. Particularly, the graphene-metal hybrid has been considered promising as a surface-enhanced Raman scattering (SERS)-active structure for biosensing applications, wherein graphene-derived chemical enhancement and metal plasmon-induced electromagnetic field enhancement are both considered the dominant mechanisms enhancing the SERS signals [16,21,27]. However, the interaction between the graphene carriers and the noble metal plasmon in the SERS process is yet to be clarified; the extruding challenge here is to identify the direction of carrier transfer

* Corresponding author. Beijing National Laboratory for Condensed Matter Physics, Institute of Physics, Chinese Academy of Sciences, Beijing 100190, China.

** Corresponding author. Beijing National Laboratory for Condensed Matter Physics, Institute of Physics, Chinese Academy of Sciences, Beijing 100190, China.

*** Corresponding author. Beijing National Laboratory for Condensed Matter Physics, Institute of Physics, Chinese Academy of Sciences, Beijing 100190, China.

E-mail addresses: jmzhao@iphy.ac.cn (J. Zhao), czgu@iphy.ac.cn (C. Gu), jjli@iphy.ac.cn (J. Li).

¹ These authors contributed equally to this work.

between the graphene and the metal, which is important to understand photosynthesis, photocatalysis, and biosensing.

Photoexcitation of metallic nanostructures (such as nanoparticles) usually leads to surface plasmonic resonances, which greatly enhance local electromagnetic fields [18,21,26]. When graphene is placed near the metallic nanostructures and excited by light, interaction between the photo-carriers in graphene and the plasmon in the metallic structure is expected. However, the details of this interaction are rarely reported, and its physical mechanism is not clear enough, especially regarding the carrier-transfer direction and its effects. This is largely because the interaction is an ultrafast process in such electronic systems, involving both single quasi-particles and collective excitations. Hence, current typical sophisticated experimental tools can barely unveil the ongoing ultrafast high temporal resolution processes with atomic- or nanoscale spatial resolution. Ultrafast optical spectroscopy is a powerful technique for temporally resolving ongoing ultrafast processes; it has potential in elucidating the carrier transfer routes by probing the ultrafast dynamics of a sample's excited states.

In the present work, we reveal the interaction between graphene carriers and the noble metal plasmon through near-infrared (IR) ultrafast dynamics spectroscopy and reveal the underlying physical mechanism by observing photo-carrier lifetimes and photo-carrier densities in the excited state. We demonstrate time-resolved ultrafast dynamics evidence that electrons are transferred from graphene to Ag nanoparticles in a graphene/Ag-NP hybrid, thereby enhancing plasmon excitation in the metallic structure and hence local electromagnetic field intensity in this system. This carrier transfer verifies graphene-mediated local field enhancement in the hybrids, which will contribute greatly to light-matter interaction, such as highly sensitive SERS processes. Specifically, the carrier transfer evidencing graphene-derived electromagnetic enhancement is also confirmed by SERS detection on Rhodamine 6G (R6G) molecules in a vertical graphene/Ag-NP hybrid structure, which exhibits unusually high sensitivity of $\sim 10^{-13}$ M for the molecules. Our investigation clarifies the role of graphene in the plasmon enhancement and electromagnetically enhanced SERS by a carrier transfer mechanism in such hybrids, which opens up new opportunities in ultrasensitive biodetection applications of graphene-plasmonic hybrid devices.

2. Experimental

2.1. Ultrafast visible-pump/IR-probe spectroscopy measurement

Our experiment employed a femtosecond amplifier laser system (Spitfire Ace, Spectra Physics) that generates laser pulses with 1 kHz repetition rate, 800 nm central wavelength, and ~ 35 fs pulse duration. The generated laser beam was split in two. One beam was frequency doubled by second-harmonic generation to generate 400 nm laser pulses. The other generated an ultra-broadband super-continuum pulse covering the mid-IR region by focusing the 800-nm fundamental light and its second harmonic in air [28]. The pulse duration of the mid-IR beam is 110 fs, and its spectrum range is $20\text{--}3500\text{ cm}^{-1}$. The 400-nm beam was the pump light, with a spot size of $400\text{ }\mu\text{m}$ on the sample surface, and the mid-IR super-continuum probe light has a spot size of $200\text{ }\mu\text{m}$. It was detected by a liquid nitrogen-cooled mercury-cadmium-telluride array detector after frequency resolution by a spectrograph. The instrumental response time is 120 fs, which has been considered in the data analysis.

2.2. Fabrication of silicon pyramid array substrate and VG/Ag-NP hybrid nanostructures

Fabrication proceeded in four steps. First, a 60-nm-thick Si_3N_4

layer was deposited on (100) silicon substrate by plasma-enhanced chemical vapor deposition. Second, a resist was spin-coated on the substrate, and an array of squares with a period of $11\text{ }\mu\text{m}$ and a side length of $9\text{ }\mu\text{m}$ was fabricated on the resist by lithography. Third, the square array pattern was transferred to the Si_3N_4 layer by reactive ion etching. Finally, a KOH solution of 20% by weight and TMAH were successively used to etch the Si at $95\text{ }^\circ\text{C}$ for 8 min in total. Thus, the array of double-layer pyramid-like structures was obtained using silicon substrate, as shown in Fig. S1(a).

The vertically standing graphene was synthesized using a home-made microwave-plasma chemical vapor deposition system. The substrates were settled on a quartz sample holder and then in a 1.2-inch quartz tube. When the pressure in the tube had been pumped down, H_2 gas was passed through to eliminate contamination in the tube. CH_4 gas was then pumped into the tube at a specific ratio with H_2 gas ($\text{CH}_4:\text{H}_2 = 75:30$ sccm). After the pressure (6 Torr) in the tube stabilized, the microwave was switched on, and plasma was generated at the entrance of the tube. The growth temperature was approximately $650\text{--}700\text{ }^\circ\text{C}$, and growth time was several minutes. After the growth process, the supply of the microwave and gas was stopped, while the tube was still pumped down, and the tube was allowed to cool down to room temperature. Then, Ag-NP with a nominal thickness of 5 nm were deposited on the vertical graphene sheets by a custom magnetron sputtering system, in which the sample holder was kept rotating at 10 rpm to ensure uniformity of deposition with a work power of 100 W and pressure of 0.004 mTorr. Scanning electron microscopy (SEM) images of as-fabricated VG/Ag-NP hybrid nanostructures are shown in Fig. S1(b)–(c).

2.3. SERS measurements

R6G was used as the Raman probe. VG/Ag-NP samples were immersed in aqueous R6G solution with a concentration of 10^{-5} M for 4 h and then repeatedly washed with DI water and dried under nitrogen. For sensitivity measurements, the solution concentration was diluted to 0.01 pM (or 10^{-14} M). SERS spectra measurements were conducted using a confocal Raman spectroscope (LabRAM HR800) equipped with a piezo stage. The excitation laser with a wavelength of 532 nm and power of 0.65 mW was focused by a $\times 100$ objective lens on the samples (see Figs. S2 and S3), and the emitted scattering signals were collected with a laser spot with a diameter of $1\text{ }\mu\text{m}$. All the samples were measured under the same conditions, and spectra were collected at 10 randomly selected pyramids on the substrate.

3. Results and discussion

Ultrafast pump-probe transient absorption spectroscopy is used to investigate the photo-carrier dynamics in a graphene/Ag-NP hybrid system by pumping in the visible range and probing in the mid-IR range. The hybrid structure is composed of a single layer of graphene covered by separated Ag-NP and is compared with pure graphene and isolated Ag-NP. Single-layer graphene grown by CVD is transferred from a Cu foil to a CaF_2 substrate. Separate Ag-NP are controllably prepared by evaporation-deposition.

In Fig. 1(a) and (b), we show ultrafast pump-probe transient absorption of the graphene/Ag-NP and pure graphene, respectively. The pump beam has a wavelength of 400 nm. The time-resolved signal is nearly independent of the probe energy, which reflects the broadband linear dispersion electronic structure of graphene in the near-IR range. Comparing Fig. 1(a) with 1(b), the lifetime of photo-carriers is significantly reduced when graphene is kept in contact with Ag-NP. To observe this clearly, we plot the absorption changes of three different samples detected at 2000 cm^{-1} (0.25 eV)

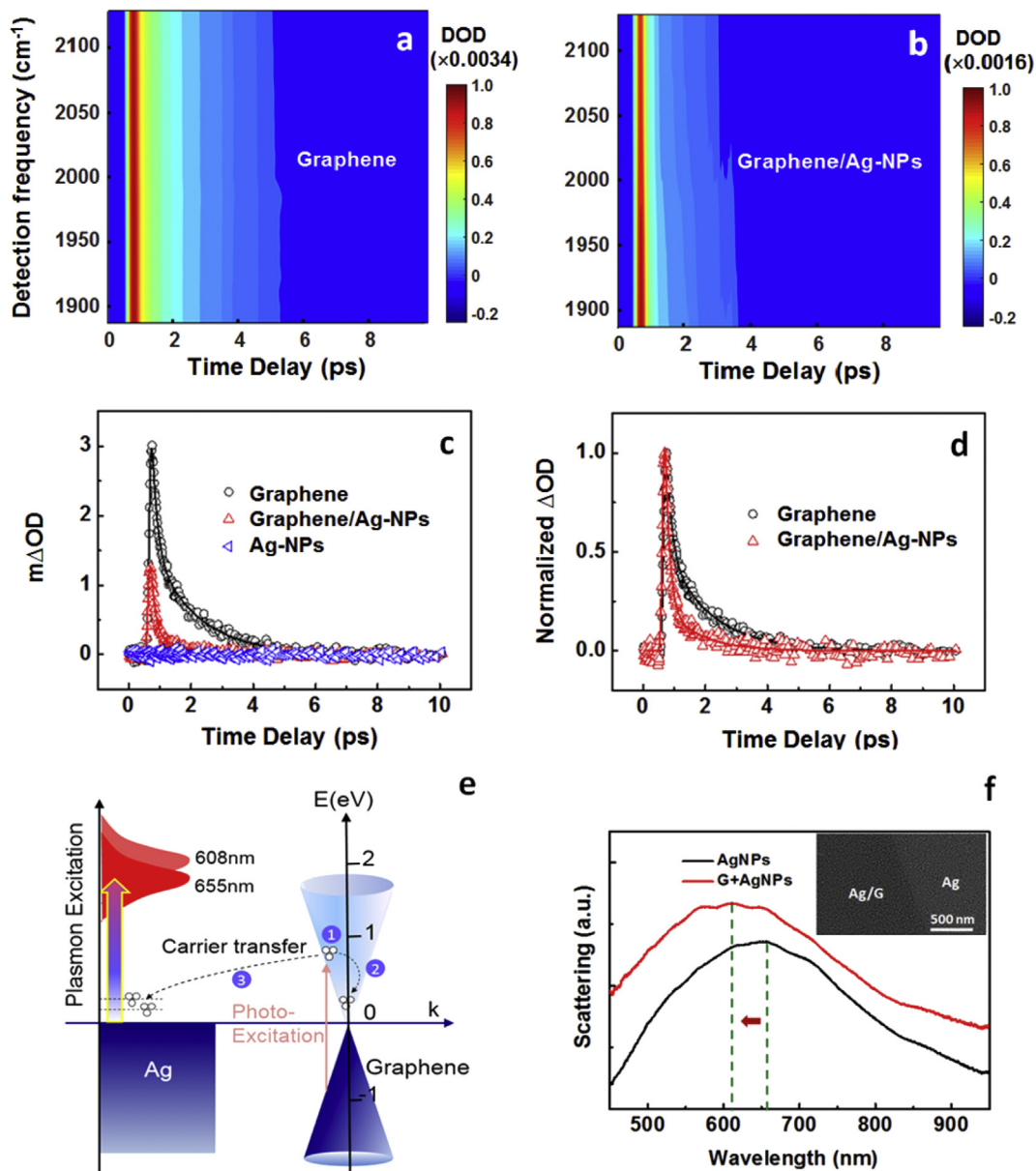


Fig. 1. Ultrafast dynamics of photo-carriers in different samples detected in the mid-infrared region. Ultrafast pump-probe transient absorption spectra of (a) graphene and (b) graphene/Ag-NP. (c) Temporal evolutions of the excitation-induced absorption changes of graphene, graphene/Ag-NP, and Ag-NP, respectively, detected at 0.25 eV. (d) Normalized photo-induced absorption changes of graphene and graphene/Ag-NP detected at 0.25 eV. Circles are experimental data and curves are multi-exponential fittings. (e) Schematic ultrafast relaxation channels of the photo-carriers, particularly including the transfer of electrons from graphene to Ag-NP. (f) Scattering spectra of the Ag-NP and graphene/Ag-NP showing the blue shift. Inset is an image of the sample measured. (A colour version of this figure can be viewed online.)

in Fig. 1(c). For the pure graphene sample, the signal exhibits two distinct exponential decays with lifetimes of 0.17 and 1.4 ps, respectively, obtained by fitting with a double-exponential function and are consistent with the results of visible light measurement [29]. We attribute the fast decay mainly to carrier-carrier scattering and the slow relaxation mainly to carrier-phonon scattering. In contrast, no prominent absorption change was detected for the Ag-NP sample, which shows very little light absorption and much shorter lifetime in this wavelength range for silver. As expected, both the amplitude and lifetime of the graphene/Ag hybrid sample are in between those of the Ag-NP and those of the graphene sample.

To compare graphene with the hybrid structure, we show the normalized transient absorption in Fig. 1(d). It can be seen that the

lifetime of graphene is significantly reduced (the quasiparticles relax back to ground state much faster) after coming in contact with Ag-NP. This is strong evidence of ultrafast charge transfer from the graphene flake to the Ag-NP. Besides the regular carrier-carrier relaxation (channel 1) and carrier-phonon scattering (channel 2), charge transfer from graphene to the Ag-NP forms a third pivotal decay channel (channel 3) for the excited-state carriers in the graphene flake of the hybrid (the three channels are marked in Fig. 1(e)). Our double-exponential fitting analysis shows two relaxation lifetimes, 0.14 and 1.1 ps, for graphene/Ag-NP. Both the fast and slow relaxations are faster than that in graphene because of this third channel through Ag-NP (Fig. 1(d)).

Important confirming evidence of charge transfer from graphene to Ag-NP also comes from observation of the amplitude.

From Fig. 1(c), it can be seen that the slow decay component has an amplitude that decreases much more than the amplitude of the fast component upon contact with the Ag-NP. Compared with that in graphene, the amplitude of the fast component decreases to 38% in the graphene/Ag-NP hybrid, while the amplitude of the slow component decreases to 14% in the hybrid. This contrasts sharply with observations of photo, thermal, and doping effects, where identical reductions are expected for both electron-electron and electron-phonon amplitudes. The prominently reduced carrier-phonon scattering can be explained only by an extra reduction of carrier density, which can be caused only by the aforementioned third decay channel—the transfer of photo-carriers from graphene to the Ag-NP. Therefore, the relative change in the amplitudes of the two components is strong evidence of the directional charge transfer from graphene to Ag-NP. If the carriers transfer from Ag to graphene, we would observe an extended carrier lifetime, which is not the case in our experiment. Our findings also demonstrate that the charge transfer is much faster than the carrier-phonon scattering in the hybrid, providing abundant extra photo-excited carriers in Ag-NP (compared with pure Ag-NP). A schematic diagram of the underlying physics is shown in Fig. 1(e), wherein the carrier transfer is marked as the third decay channel. Similar extra decay channels have also been investigated for phonon systems [30].

Given the two direct ultrafast spectroscopy evidence of the charge transfer above, it is reasonable to expect that the hybrid may possess greater plasmon excitability than the Ag-NP alone. As the carrier density in the hybrid system is enhanced, the plasmon frequency is expected to undergo a blue-shift. To further verify our arguments presented in the above two paragraphs, we performed a control experiment, the scattering spectrum, for the Ag-NP and graphene/Ag-NP. The results are shown in Fig. 1(f), which clearly demonstrates that the central peak position of the plasmon resonance is blue-shifted from 655 to 608 nm because of contact with graphene. This unambiguously indicates that the carriers transfer from graphene to Ag-NP, instead of the converse. This is exactly as we expected: if the carriers were to transfer from the Ag-NP to graphene, a red-shift should be observed, which is not the case. This control experiment also excludes the possibility that impurities or defect states form and dominate the charge transfer mechanism (by forming a different third decay channel). The blue-shift reveals that the transferred carriers mainly join the plasmon excitations, rather than impurities or defects. We designate this control experiment of scattering spectrum as the third body of evidence that charge transfer occur from graphene to the Ag-NP.

Therefore, the above results and discussions progressively clarify the physical process that graphene behaves as an electron reservoir and transfers carriers to the Ag-NP when light excites the hybrid structure and whose carrier density increases, thus directly enhancing the plasmon therein. Here the high carrier mobility and broadband linear dispersion of graphene contribute to enabling it as an electron reservoir. We conjecture that this plasmon enhancement generates a very strong local electromagnetic field, which can lead to various important light-matter interactions for a variety of applications such as SERS, which is one of such light-matter interactions. If our above overall interpretation is correct, it can be expected to see graphene-mediated local-field-enhanced SERS in this hybrid structure, which is more prominent than that in pure metal or graphene structures. To verify this, we design a SERS experiment using our graphene/Ag-NP nanostructure. More importantly, we hope that carrier transfer from graphene to Ag-NP in such hybrid can attest to the fact that graphene contributes greatly to the electromagnetic enhancement besides chemical enhancement in SERS.

To fully verify the role of graphene-enhanced plasmon in local field-enhanced SERS, a three-dimensional plasmonic hybrid of

graphene/Ag-NP is fabricated on a Si pyramid array (see Fig. S1) for SERS measurement. The structure consists of a large area of vertical graphene nanosheets (VGs) covered with Ag-NP on the surface of the array of Si pyramids. An SEM image of the VG/Ag-NP hybrid on a single pyramid is shown in Fig. 2(a), clearly displaying the sheet-like morphology of the VGs and their high-density distribution. A single graphene sheet is located vertically on the pyramid apex, and three enlarged images are displayed below Fig. 2(a), corresponding to the morphologies of the same single graphene sheet before and after coating Ag-NP; this indicates that Ag-NPs are coated uniformly on both sides of this graphene sheet with sizes of about 15 nm and an average interval of 3 nm. More details of the fabrication process are described in the Experimental Section. In addition, the Raman spectra characterization of VGs demonstrates that the ratio of the G band intensity to 2D band intensity is nearly 1, suggesting that the as-grown vertical graphene must be few layers (2–3 layer) [31], as depicted in Fig. S2. In addition, the homogeneous distribution and stability of the Ag-NP on the graphene sheets depend on surface diffusion coefficient of Ag on the graphene and surface diffusion barrier between Ag and graphene [32]. Compared with monolayer graphene, our as-grown few-layer graphene sheets have lower surface diffusion barrier and higher surface diffusion coefficient for Ag, resulting in easier motion of Ag atom along the graphene surface; this property favors uniform distribution and high density nucleation for Ag particles [33]. This homogeneous distribution also augments the stability of the Ag-NP on the graphene sheets.

For the VG/Ag-NP hybrids, SERS measurements are performed under an excitation wavelength of 532 nm, and R6G, a frequently used fluorescent dye molecule, is used as the probe to determine the SERS properties of the hybrid nanostructures. Fig. 2(b) shows the SERS spectra of R6G with different Raman signal enhancements from three kinds of substrates: pure Ag-NP, pure VGs, and VG/Ag-NP hybrid nanostructures. As shown in Fig. 2(b), the pure VGs, similar to the flat graphene, constitute a chemically enhancing substrate, and its Raman enhancement effect is rather weaker than that of pure Ag-NPs; this occurs due to electromagnetic field enhancement. The VG/Ag-NP hybrid exhibits the best performance in the Raman signal enhancement among the three SERS substrates, and its Raman signal is far stronger than those of the other two substrates. According to one widely held view, besides the graphene-derived chemical enhancement of SERS, the greatly enhanced SERS is attributable mainly to a large quantity of Ag-NP located on the vertical graphene sheets, having a large specific surface area that can produce high-density “hot-spots” providing intense field enhancement. However, from our result (Fig. 2), we know that a large quantity of Ag-NP alone is inadequate to enhance the Raman signal so much; thus, it is conceivable that graphene-mediated local electromagnetic field enhancement also contributes significantly to the enhanced SERS in the hybrid nanostructures. This finding is in accord with the above conclusion that ultrafast electron transfer from graphene to Ag-NP induced giant electromagnetic enhancement to contribute to SERS.

Graphene-induced electric field enhancement in the VG/Ag-NP hybrid system is also demonstrated by a finite-difference time-domain (FDTD) simulation for a 532-nm-wavelength incident light. To simplify, only a single Ag-NP in contact with graphene is considered, which is simplified as having a mooncake shape, with a long oval cross-section. Fig. 2(c) shows X-Z views of the electric field amplitude distribution in both Ag-NP/CaF₂ and Ag-NP/graphene/CaF₂, corresponding to the first sample used for ultrafast pump-probe transient absorption measurements. Comparing Ag-NP/CaF₂ with Ag-NP/graphene/CaF₂, a stronger field enhancement clearly appears in between Ag-NP and graphene, as well as at both sides of Ag-NP, indicating graphene's enhancement of local field

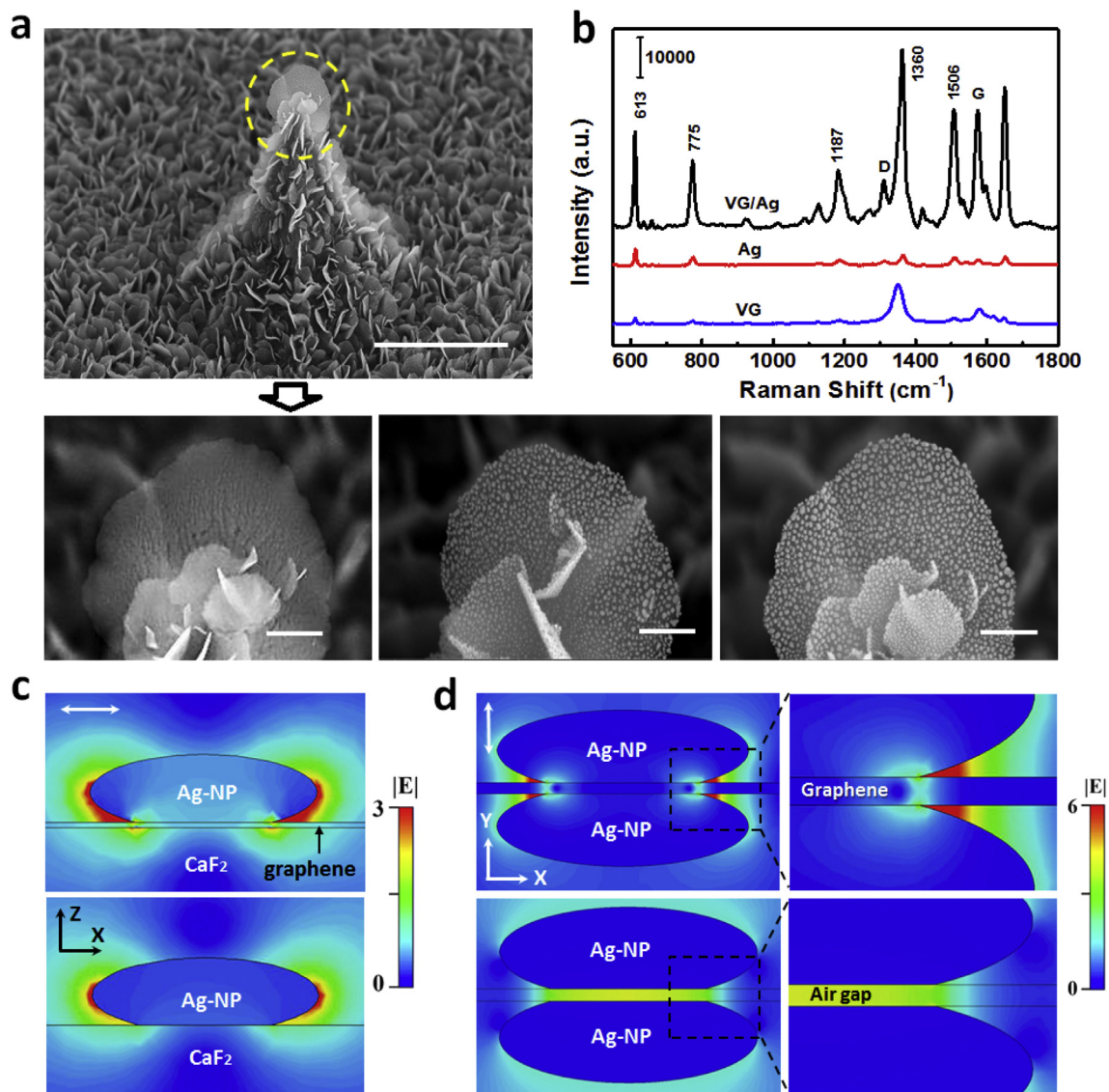


Fig. 2. (a) SEM image of VG/Ag-NP hybrid on Si pyramid. A single sheet located vertically on the pyramid apex is marked by a yellow dotted line, and its enlarged views are shown below, including the front side of a single sheet on the apex (right), its back side (middle), and uncoated Ag-NP (left) on the same VG at the apex of the Si pyramid. Scale bar, 2 μm and 200 nm. (b) SERS spectra of R6G on different substrates: pure Ag-NP, pure VGs, and VG/Ag-NP hybrid. The wavelength of the incident light is 532 nm. The white arrow indicates polarization of the incident light. A single Ag-NP is modeled to be mooncake-like, 15 nm in diameter and 5 nm in thickness. (c) X-Z view of the electric field distribution of Ag-NP/CaF₂ and Ag-NP/graphene/CaF₂, respectively. (d) X-Y view of the electric field distribution of Ag-NP/bilayer-graphene/Ag-NP and Ag-NP/air-gap/CaF₂, where the width of air gap is equal to the thickness of bilayer graphene. The right junctional zone is enlarged for a clearer view of the electric field distribution. (A colour version of this figure can be viewed online.)

intensity in the hybrid system. Fig. 2(d) shows the X-Y views of the electric field amplitude distribution of Ag-NP/bilayer graphene/Ag-NP, corresponding to the sample of VG/Ag-NP hybrid used for SERS measurements. To compare with Ag-NP/bilayer-graphene/Ag-NP, the bilayer-graphene is replaced with an air-gap with equal thickness to form a model of Ag-NP/air-gap/Ag-NP. The simulation results show that the highest value of field intensity in the junction region of Ag-NP/bilayer-graphene/Ag-NP is approximately one order of magnitude larger than that of Ag-NP/air-gap/Ag-NP. Thus, the addition of graphene greatly enhances the local field intensity in the plasmonic hybrid by graphene-plasmon interaction and is expected to be the dominant contributor to the detected Raman signal. The above FDTD result agrees well with our prediction of graphene-mediated local field enhancement for SERS applications.

Owing to the essential role of graphene in greatly enhancing SERS, arising from carrier-transfer enhanced charge density by

touching the carrier reservoir, we naturally expect that ultrahigh sensitivity can be realized in such a VG/Ag-NP hybrid system, which is crucial for SERS sensor applications. To further optimize SERS measurement, a 5-nm-thick Ag film coating on the VGs is chosen for our experiment in ultrasensitive SERS detection because it shows the strongest Raman signal in Fig. 3(a). To obtain the sensitivity of the hybrid structure as a SERS substrate, Raman spectra of R6G molecules with concentrations from 10^{-6} to 10^{-14} M on the hybrid substrate are successively measured, as shown in Fig. 3(b) and (c); this substantially demonstrates the capability of the hybrid nanostructures on silicon pyramids to serve as an ultrasensitive SERS substrate. The two characteristic Raman shift peaks of R6G molecules centered at 613 and 775 cm^{-1} keep a sharp intensity at the R6G molecule concentration from 10^{-11} to 10^{-12} . Especially when the R6G aqueous solution is diluted to 10^{-13} M, two characteristic Raman shift peaks of R6G molecules are clearly

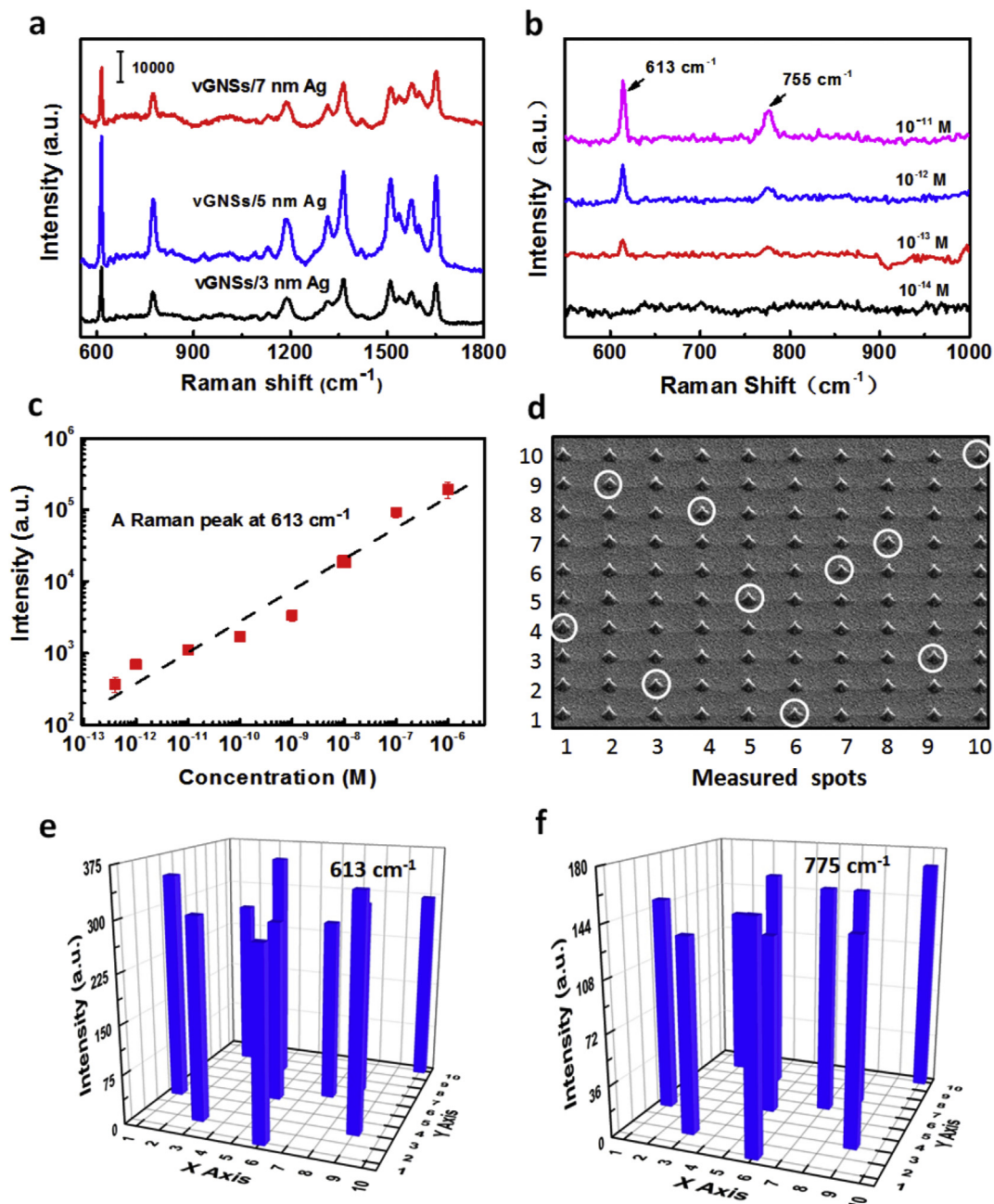


Fig. 3. (a) SERS spectra of R6G from VG/Ag-NP hybrid nanostructures on Si pyramids with different thicknesses of Ag-NP. (b) Enlarged SERS spectra at low molecular concentrations from 10^{-11} to 10^{-14} M, including two characteristic Raman shift peaks of R6G molecule centered at 613 and 775 cm^{-1} . (c) The intensity of the Raman feature peak of the R6G at 613 cm^{-1} as a function of molecular concentration, from 10^{-6} to 10^{-14} M (in log scale). (d) SEM image showing the 10 randomly selected measuring positions on a 10×10 array of the hybrid nanostructures for SERS detection at an ultralow concentration of 10^{-13} M. (e–f) The intensity of the feature peaks at 613 and 775 cm^{-1} in SERS spectra of R6G is tested on the 10 selected measured positions corresponding to (d) for uniformity of measurement. (A colour version of this figure can be viewed online.)

distinguishable—a dilute concentration that was seldom reported detectable in previous literature, fully reflecting ultrasensitive molecule detection ability, as shown in Fig. 3(b). Fig. 3(c) indicates the change in intensity of the characteristic Raman shift peak at 613 cm^{-1} with the concentration of R6G molecules declining from 10^{-6} to 10^{-14} M and reveals a linear dependence of intensity on the concentration of R6G molecules.

For the evaluation of SERS measurement sensitivity, uniformity is also a very important characteristic, which poses great challenges to the SERS substrate, especially at an ultralow molecular concentration with accurate localization measurement. Here, a SERS substrate of

VG/Ag-NP hybrid nanostructures on 10×10 pyramids in both horizontal and vertical directions (nearly $110 \mu\text{m}^2$) is chosen to demonstrate the measurement uniformity (Fig. 3(d)). Ten points (i.e. pyramids) throughout the area are then randomly chosen as SERS measuring spots, marked by white circles in Fig. 3(d). An ultralow concentration of 10^{-13} M is used. The uniformity of SERS spectra of R6G is measured from the 10 random points, and the intensity distribution of the two characteristic peaks at 613 and 775 cm^{-1} corresponding to the 10 tested points are presented in Fig. 3(e) and (f), respectively. Comparing the 10 points, the average deviation in peak intensity is about 7% at both 613 and 775 cm^{-1} , indicating reasonable

uniformity of the SERS signal in the region. In addition, the stability of substrate is a very important characteristic for the evaluation of SERS measurement. In this work, our VG/Ag-NP samples as SERS substrate are kept in a vacuum of 10^{-4} Pa to avoid oxidization before SERS measurement. We tested and found that these samples remain stable for SERS measurements even after 10 days.

Furthermore, this sample of VG/Ag-NP on Si pyramids also performs as an addressable sensor chip, which exhibits ultrasensitive (as high as 10^{-13} M) SERS detection. The statistical data and comparison results of the 10 randomly selected detection points from a 10×10 array also shows good uniformity and repeatability of the hybrid SERS substrates. The array of micrometer-sized Si pyramids enables to accurately locate the measured positions. Thus, the ultrasensitive SERS detection ability of the VG/Ag-NP hybrid is demonstrated. It depends on intense interaction between graphene and Ag-NP and particularly the prominent carrier transfer from graphene to Ag-NP that greatly contributes to the electromagnetic enhancement in SERS. In addition, compared with other reported graphene-oxide (GO)–Ag or reduced graphene-oxide (RGO)–Ag hybrid substrates [34,35], our vertical few-layer graphene/Ag-NP hybrid substrate exhibited a better SERS efficiency. The as-grown graphene has a big advantage over GO and RGO because the large quantities of defects and poor conductivity in GO and RGO will degrade the carrier transfer and hence the capability of SERS detection. Our few-layer graphene/Ag-NP hybrids are also superior to other reported graphene-Ag hybrids because of a large specific surface area carrying abundant Ag-NP that can produce high-density “hot-spots” effect [36].

4. Conclusions

In conclusion, we have presented clear evidence of ultrafast carrier transfer from graphene to Ag-NP, wherein the graphene acts as a carrier reservoir in the graphene/Ag-NP hybrids. We propose an underlying physical mechanism for the carrier-plasmon interaction wherein carrier transfer forms a third pivotal decay channel for the excited quasiparticles in addition to the two regular channels (carrier-carrier relaxation and carrier-phonon scattering) in the hybrid system. This ultrafast process of the carriers in such plasmonic nanostructures leads to graphene-derived giant local field enhancement and verifies the pivotal role of graphene in plasmon enhancement for such hybrids, which provides a foundation that supports a plethora of future hybrid nanostructure designs, especially those for SERS sensor applications. Further, we demonstrate that graphene electromagnetically enhanced the ultrasensitive SERS process (as high as 10^{-13} M) by a vertical few-layer graphene/Ag-NP hybrid plasmonic array on a Si pyramid substrate. Our experimental clarification of the ultrafast carrier transfer route, the underlying physical mechanism of graphene-induced local electromagnetic enhancement, and the great contribution of graphene to electromagnetically enhanced SERS in graphene/Ag-NP hybrid widens the way for designing and implementing ultrasensitive SERS, chemical or biological sensors, etc.

Acknowledgments

This work is supported by the National Key Research and Development Program of China (2016YFA0200800, 2016YFA0200400 and 2016YFB010050), the National Natural Science Foundation of China (Grant Nos. 91323304, 11674387, 61390503, 11574369, 11574383, 91436102, 21603270), and the Strategic Priority Research Program of the Chinese Academy of Sciences (Grant No. XDB07020200). The authors would like to thank Prof. Y. C. Fan of Northwestern Polytechnical University for helpful discussion on FDTD simulation.

Appendix A. Supplementary data

Supplementary data related to this article can be found at <http://dx.doi.org/10.1016/j.carbon.2017.05.076>.

References

- [1] M. Kahl, E. Voges, Analysis of plasmon resonance and surface-enhanced Raman scattering on periodic silver structures, *Phys. Rev. B* 61 (20) (2000) 14078–14088.
- [2] A.N. Grigorenko, M. Polini, K.S. Novoselov, Graphene plasmonics, *Nat. Phot.* 6 (11) (2012) 749–758.
- [3] X. Liang, T. You, D. Liu, X. Lang, E. Tan, J. Shi, P. Yin, L. Guo, Direct observation of enhanced plasmon-driven catalytic reaction activity of Au nanoparticles supported on reduced graphene oxides by SERS, *Phys. Chem. Chem. Phys.* 17 (15) (2015) 10176–10181.
- [4] F. Guinea, M.I. Katsnelson, A.K. Geim, Energy gaps and a zero-field quantum Hall effect in graphene by strain engineering, *Nat. Phys.* 6 (1) (2010) 30–33.
- [5] R. Wu, Y.L. Zhang, S.C. Yan, F. Bian, W.L. Wang, X.D. Bai, X.H. Lu, J.M. Zhao, E.G. Wang, Purely coherent nonlinear optical response in solution dispersions of graphene sheets, *Nano Lett.* 11 (12) (2011) 5159–5164.
- [6] Y.C. Tian, H. Tian, Y.L. Wu, L.L. Zhu, L.Q. Tao, W. Zhang, Y. Shu, D. Xie, Y. Yang, Z.Y. Wei, X.H. Lu, T. Ren, C. Shih, J.M. Zhao, Coherent generation of photo-thermo-acoustic wave from graphene sheets, *Sci. Rep.* 5 (2015), 10582–10582.
- [7] P.G. Song, Z.H. Cao, Y.Z. Cai, L.P. Zhao, Z.P. Fang, S.Y. Fu, Fabrication of exfoliated graphene-based polypropylene nanocomposites with enhanced mechanical and thermal properties, *Polymer* 52 (18) (2011) 4001–4010.
- [8] A.K. Geim, K.S. Novoselov, The rise of graphene, *Nat. Mater.* 6 (3) (2007) 183–191.
- [9] T. Zhang, Q.Z. Xue, S. Zhang, M.D. Dong, Theoretical approaches to graphene and graphene-based materials, *Nano Today* 7 (3) (2012) 180–200.
- [10] S. Barraza-Lopez, Coherent electron transport through freestanding graphene junctions with metal contacts: a materials approach, *J. Comp. Elec.* 12 (2) (2013) 145–164.
- [11] Y. Zhao, W. Zeng, Z. Tao, P. Xiong, Y. Qu, Y. Zhu, Highly sensitive surface-enhanced Raman scattering based on multi-dimensional plasmonic coupling in Au-graphene-Ag hybrids, *Chem. Comm.* 51 (5) (2015) 866–869.
- [12] J. Zhao, M.T. Sun, Z. Liu, B.G. Quan, C.Z. Gu, J.J. Li, Three dimensional hybrids of vertical graphene-nanosheet sandwiched by Ag-nanoparticles for enhanced surface selectively catalytic reactions, *Sci. Rep.* 5 (2015) 16019.
- [13] A.M. Gilbertson, Y. Francescato, T. Roschuk, V. Shahtsova, Y. Chen, T.P. Sidiropoulos, M. Hong, V. Giannini, S.A. Maier, L.F. Cohen, R.F. Oulton, Plasmon-induced optical anisotropy in hybrid Graphene–Metal nanoparticle systems, *Nano Lett.* 15 (5) (2015) 3458–3464.
- [14] A. Hoggard, L.Y. Wang, L.L. Ma, Y. Fang, G. You, J. Olson, Z. Liu, W. Chang, P.M. Ajayan, S. Link, Using the plasmon linewidth to calculate the time and efficiency of electron transfer between gold nanorods and graphene, *ACS Nano* 7 (12) (2013) 11209–11217.
- [15] Z. Dai, X. Xiao, W. Wu, Y. Zhang, L. Liao, S. Guo, J. Ying, C. Shan, M. Sun, C. Jiang, Plasmon-driven reaction controlled by the number of graphene layers and localized surface plasmon distribution during optical excitation, *Light Sci. Appl.* 4 (10) (2015) e342.
- [16] X. Li, W. C. H. Choy, X. G. Ren, D. Zhang, H. F. Lu, Highly intensified surface enhanced raman scattering by using monolayer graphene as the nanopacer of metal film–metal nanoparticle coupling system. *Adv. Func. Mater.* 24(21) (014) 3114–3122.
- [17] X. Ling, L.M. Xie, Y. Fang, H. Xu, H.L. Zhang, J. Kong, M.S. Dresselhaus, J. Zhang, Z.F. Liu, Can graphene be used as a substrate for raman enhancement? *Nano Lett.* 10 (2) (2010) 553–561.
- [18] Z. Hu, Z. Liu, L. Li, B. Quan, Y. Li, J. Li, C. Gu, Wafer-scale double-layer stacked Au/Al₂O₃/Au nanosphere structure with tunable nanospacing for surface-enhanced raman scattering, *Small* 10 (19) (2014) 3933–3942.
- [19] K.F. Mak, M.Y. Sfeir, Y. Wu, C.H. Liu, J.A. Misewich, T.F. Heinz, Measurement of the optical conductivity of graphene, *Phys. Rev. Lett.* 101 (19) (2008), 196405.
- [20] Y.L. Wu, Q. Wu, F. Sun, C. Cheng, S. Meng, J.M. Zhao, Emergence of electron coherence and two-color all-optical switching in MoS₂ based on spatial self-phase modulation, *Proc. Nat. Acad. Sci.* 112 (38) (2015) 11800–11805.
- [21] P. Wang, O. Liang, W. Zhang, T. Schroeder, Y. Xie, Ultra-sensitive graphene-plasmonic hybrid platform for label-free detection, *Adv. Mater.* 25 (35) (2013) 4918–4924.
- [22] L.M. Xie, X. Ling, Y. Fang, J. Zhang, Z.F. Liu, Graphene as a substrate to suppress fluorescence in resonance raman spectroscopy, *J. Am. Chem. Soc.* 131 (29) (2009) 9890–9891.
- [23] W.G. Xu, X. Ling, J.Q. Xiao, M.S. Dresselhaus, J. Kong, H.X. Xu, Z.F. Liu, J. Zhang, Surface enhanced Raman spectroscopy on a flat graphene surface, *Proc. Nat. Acad. Sci.* 109 (24) (2012) 9281–9286.
- [24] N. Papisimakis, Z.Q. Luo, Z.X. Shen, F.D. Angelis, E.D. Fabrizio, A.E. Nikolaenko, N.I. Zheludev, Graphene in a photonic metamaterial, *Opt. Exp.* 18 (8) (2010) 8353–8359.
- [25] Y.L. Wu, L.L. Zhu, Q. Wu, F. Sun, J.K. Wei, Y.C. Tian, W.L. Wang, X.D. Bai, X. Zuo, J.M. Zhao, Electronic origin of spatial self-phase modulation: evidenced by comparing graphite with C60 and graphene, *Appl. Phys. Lett.* 108 (24) (2016),

- 241110.
- [26] J. Zhao, W. Sun, W. Sun, L. Liu, X. Xia, B. Quan, A. Jin, C. Gu, J. Li, Rapid templated fabrication of large-scale, high-density metallic nanocone arrays and SERS applications, *J. Mater. Chem. C* 2 (46) (2014) 9987–9992.
- [27] R.T. Lu, A. Konzelmann, F. Xu, Y.P. Gong, J.W. Liu, Q.F. Liu, M. Xin, R.Q. Hui, J.Z. Wu, *Carbon* 86 (2015) 78–85Crossref.
- [28] J.M. Dawlaty, S. Shivaraman, M. Chandrashekar, Photogenerated intrinsic free carriers in small-molecule organic semiconductors visualized by ultrafast spectroscopy, *Sci. Rep.* 5 (2015) 17076.
- [29] J.M. Dawlaty, S. Shivaraman, M. Chandrashekar, Measurement of ultrafast carrier dynamics in epitaxial graphene, *Appl. Phys. Lett.* 92 (4) (2008) 42116.
- [30] Y.C. Tian, W.H. Zhang, F.S. Li, Y.L. Wu, Q. Wu, F. Sun, G.Y. Zhou, L. Wang, X. Ma, Q.K. Xue, J. Zhao, Ultrafast dynamics evidence of high temperature superconductivity in single unit cell FeSe on SrTiO₃, *Phys. Rev. Lett.* 116 (2016) 107001.
- [31] L.L. Jjiang, T.Z. Yang, F. Liu, J. Dong, Z.H. Yao, C.M. Shen, S.Z. Deng, N.S. Xu, Y.Q. Liu, H.-J. Gao, Controlled synthesis of large-scale, uniform, vertically standing graphene for high-performance field emitters, *Adv. Mater* 25 (2) (2013) 250–255.
- [32] Z.T. Luo, L.A. Somers, Y.P. Dan, T. Ly, N.J. Kybert, E.J. Mele, A.T.C. Johnson, *Nano Lett.* 10 (2010) 777.
- [33] H.Q. Zhou, C.Y. Qiu, F. Yu, H.C. Yang, M.J. Chen, L.J. Hu, L.F. Sun, *J. Phys. Chem. C* 115 (2011) 11348–11354.
- [34] W. Fan, Y.H. Lee, S. Pedireddy, Q. Zhang, T.X. Liu, X.Y. Ling, *Nanoscale* 6 (2014) 4843–4851.
- [35] G. Lu, H. Li, C. Liusman, Z.Y. Yin, S.X. Wu, H. Zhang, *Chem. Sci.* 2 (2011) 1817–1821.
- [36] R. Goul, S. Das, Q.F. Liu, M. Xin, R.T. Lu, R. Hui, J.Z. Wu, *Carbon* 111 (2017) 386–392.